Available online at www.sciencedirect.com
SCIENCE DIRECT®
Journal of Power Sources 143 (2005) 243–255
JOURNAL OF POWER SOURCES
www.elsevier.com/locate/jpowsour

The structure and electrochemical performance of spherical Al-substituted α-$Ni(OH)_2$ for alkaline rechargeable batteries

H. Chen[a], J.M. Wang[a,*], T. Pan[a], Y.L. Zhao[a], J.Q. Zhang[a,b], C.N. Cao[a,b]

[a] *Department of Chemistry, Zhejiang University, Hangzhou 310027, PR China*
[b] *Chinese State Key Laboratory for Corrosion and Protection, Shenyang 110015, PR China*

Received 26 November 2003; received in revised form 8 November 2004; accepted 16 November 2004
Available online 15 January 2005

Abstract

Spherical Al-substituted α-$Ni(OH)_2$ for alkaline rechargeable batteries was prepared by a complexation-coprecipitation method. The morphology and structure of the samples were characterized by SEM, XRD and Raman spectroscopy. Their electrochemical performance including charge–discharge behavior, diffusion coefficient of proton (D_{H^+}), stability in strong alkaline solution and cycle life was also investigated. The results showed that the Al-substituted α-$Ni(OH)_2$ prepared by this method manifests perfect spherical shape and the specific discharge capacity of the sample with 18.3 mol% Al reaches 477 mAh g^{-1} when the pH value of synthesis solution is 11.75. The interlayer distance, the oxygen evolution potential and the half discharge potential of the sample increase greatly with the increase of Al content. Compared with β-$Ni(OH)_2$ without Al substitution, there are large amounts of proton defects in Al-substituted α-$Ni(OH)_2$ which increases the diffusion coefficient of proton (D_{H^+}) measured by current pulse relaxation (CPR). The Al-substituted α-$Ni(OH)_2$ sample shows an excellent structural stability during ageing treatment in 6 M KOH solution and the loss of Al can be neglected.

Keywords: Spherical Al-substituted α-$Ni(OH)_2$; Electrochemical performance; Structure

1. Introduction

Nickel hydroxide has been widely used as the positive electrode material of Ni–Cd, Ni–Fe, Ni–Zn, Ni–H_2 and Ni–MH rechargeable batteries. In commercial batteries, spherical β-$Ni(OH)_2$ powders are usually utilized since it has a high tapping density (>2.0 g cm^{-3}) and good stability in strong alkaline electrolyte. However, there are two factors that inhibit its further improvement as the active material [1]: (i) the theoretical capacity of β-$Ni(OH)_2$ is 289 mAh g^{-1} due to one electron transportation in β-$Ni(OH)_2$/β-NiOOH system, which has been approximately reached in the present commercial batteries. (ii) γ-NiOOH is easily formed when β-$Ni(OH)_2$ is overcharged, which results in a swelling of the positive electrode volume by the intercalation of water molecules and metallic cation such as K^+ and causes a rapid capacity fading during charge/discharge cycles.

Recently, more attention has been paid on α-$Ni(OH)_2$. For α-$Ni(OH)_2$/γ-NiOOH couple, larger discharge capacity can be obtained since the oxidation state of nickel in γ-NiOOH is 3.67 or 3.3–3.7 [2,3] and there are no volume expansion and mechanical deformation problems. However, pure α-$Ni(OH)_2$ is labile in strong alkaline medium and easily transforms to β-$Ni(OH)_2$ [1]. Many efforts have been focused on the preparation of stabilized α-$Ni(OH)_2$ by partial substitution of Co [4], Al [5–10], Fe [11], Mn [12] and Zn [13,14] for Ni to increase the stability of α-phase structure in strong alkaline medium. In addition to increasing stability of α-phase, Co and Mn substitutions are found to decrease the electrode potential, whereas, Fe and Al substitution causes an increase. Aluminum is considered to be the most effective element to stabilize α-$Ni(OH)_2$ and improve its electrochemical performance. Kamath et al. [5] chemically pre-

* Corresponding author. Tel.: +86 571 87951513; fax: +86 571 87951895.
E-mail address: cncao@sun.zju.edu.cn (J.M. Wang).

0378-7753/$ – see front matter © 2004 Elsevier B.V. All rights reserved.
doi:10.1016/j.jpowsour.2004.11.041

pared the Ni/Al-LDHs with specific discharge capacity of 240 mAh g^{-1} and half discharge potential of 350 mV (versus Hg/HgO) for a 20 mol% Al-containing compound. Wei-Kang Hu and Noreus [10] recently reported that the α-phase nickel hydroxide with a 10 mol% Al content gained a stable capacity of 320 mAh g^{-1} and had satisfactory stability in 6.0 M KOH and during electrochemical cycling for 300 cycles. Although the stability has been improved greatly, the electrochemical performance (activation, electrode potential, etc.) and the dynamic mechanism of Al-substituted α-$Ni(OH)_2$ have not been studied in detail. The usual synthesis method is adding a mixed metal-nitrate solution containing Ni and Al to NaOH or LiOH solution with stirring [5–7]. The obtained α-$Ni(OH)_2$ often shows irregular shape and bad fluidness.

In the present work, Al-substituted α-$Ni(OH)_2$ was prepared by a complex-coprecipitation method. The effects of pH value and Al content on the physical properties and electrochemical performance of α-$Ni(OH)_2$ are investigated in detail.

2. Experimental

2.1. Preparation of active material

A solution of $NiSO_4$ (1.0 M) complexed with aqueous ammonia and a mixed solution of NaOH (2.4 M) containing $Al_2(SO_4)_3$ (in a required $[Ni^{2+}]/([Al^{3+}]+[Ni^{2+}])$ ratio), Na_2CO_3(2.5 g dm^{-3}) and aqueous ammonia (1.0 M) were slowly added to a well-sealed reaction vessel with 250 mL aqueous ammonia solution (1.0 M) at the same feeding speed with vigorous stirring. Reaction temperature was controlled at 55 ± 1 °C, and the pH value of reaction solution was held at 11.0–12.25. After the precipitation reaction had been undertaken for 6–8 h, the reaction product was aged in mother solution for another 16 h at 55 °C. The product was filtered off, washed several times with deionized water to neutral, and dried at 60 °C in air.

2.2. Characterization of nickel hydroxide

The chemical compositions (Ni) of the samples were obtained using an atomic absorption spectrophotometer (AAS) (model 180-50 from Hitachi) and the Al contents were measured by an inductively coupled argon plasma emission spectrophotometer (ICP, IRIS Intrepid II XSP, Thermo Electron Corporation, USA). The tapping density of the samples was measured by following method: a certain amount of sample was put into a measuring cylinder and was knocked to a constant volume. Dividing the mass of the sample by its tapping volume is the tapping density.

The structure of the samples were determined using X-ray diffractometer (Rigaku D/Max 2550), Cu Kα radiation at 40 kV, 300 mA. The morphology of the samples was examined using scanning electron microscopy (SEM) (Philiphs XL 30 ESEM). The nickel hydroxide powders were also studied by Almega Dispersive Raman Spectroscopy (Thermo Nicolet company) and the wavelength of laser is 532 nm.

2.3. Preparation of electrodes and electrochemical tests

The pasted nickel electrodes were prepared as follows: 90 wt.% sample, 5 wt.% cobalt powder and 5 wt.% graphite powder were thoroughly mixed with a certain amount of 5% PTFE solution. The paste obtained was incorporated into nickel foam (2 cm × 2 cm × 0.9 mm) with a spatula. The pasted nickel electrodes were dried at 50 °C and then roll-pressed to thickness of 0.5 mm. Thereafter, the electrodes were soaked in 6 M KOH for 24 h before being coupled with porous Ni electrodes on either side as counters and a Hg/HgO electrode as reference. Galvanostatic charge–discharge studies were conducted using a DC-5 cell performance-testing instrument (made in China). The working electrode was galvanostatically charged at 0.1 C rate for 15 h, rest for 5 min, and then discharged to 0.1 V versus Hg/HgO at 0.1 C rate for five activation cycles. Cycle performance was tested under the following scheme: charge at 1.0 C rate for 1.4 h, rest for 5 min, and discharge at 1.0 C rate to 0.1 V versus Hg/HgO.

The proton diffusion coefficient (D_{H^+}) in nickel electrodes was measured by the current–pulse relaxation (CPR) technique described by Kumagai and coworkers [15–17] using the following formula for the time dependence of the transient potential (ΔE):

$$\Delta E = IV_m\tau(dE/dn)/FA(\pi D_{H^+}t)^{1/2} \quad (1)$$

where I is a current pulse (300 mA), V_m the molar volume (31.83 and 22.61 cm^3 for α-$Ni(OH)_2$ and β-$Ni(OH)_2$, respectively [16,17]), τ the duration of the pulse (8 s), (dE/dn) the slope of the open-circuit potential (OCP) as a function of capacity, and A the apparent geometric area (4 cm^2), which is assumed to be true in the present work. The equilibrium open-circuit potential (OCP) was measured after about 24 h on open-circuit. In Eq. (1), n = 0–1.5 is used by assuming the following electrode reaction:

$$NiOOH_x \leftrightarrow NiOOH_{x-n} + nH^+ + ne^-(x = 0\text{–}2, n = 0\text{–}2) \quad (2)$$

These CPR tests were conducted on the Arbin BT-2000 system. All the electrochemical tests were carried out at room temperature.

3. Results and discussion

3.1. Effects of pH value on the physical properties and initial discharge capacity

The Al-substituted α-nickel hydroxide was synthesized via an aqueous solution complexation-coprecipitation route. The formation reactions of $Ni(OH)_2$ powders are as follows:

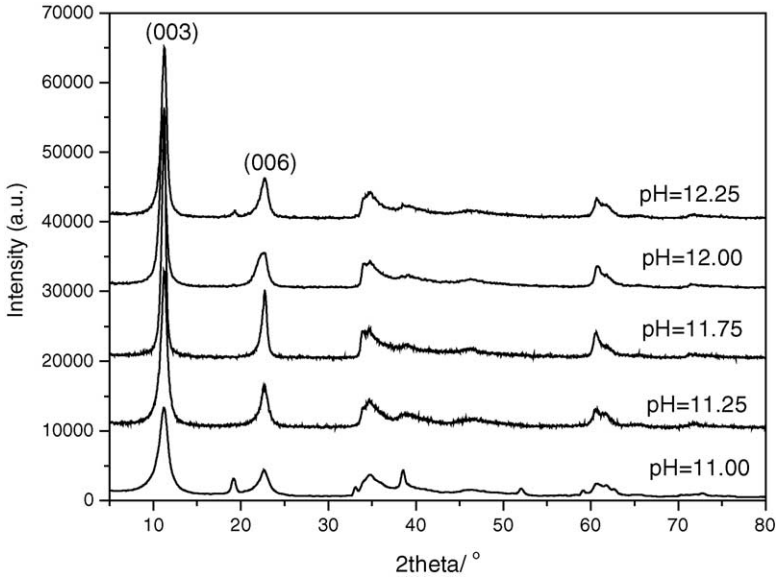

Fig. 1. XRD patterns of Al-substituted α-$Ni(OH)_2$ samples (Al 20%)synthesized at different pH values.

$$[Ni(NH_3)_6]^{2+}{}_{(aq)} + 2OH^- + 6H_2O \rightarrow Ni(OH)_{2(s)} + 6NH_4OH_{(aq)} \quad (3)$$

$$AlO_2{}^- + 2H_2O \rightarrow Al(OH)_{3(s)} + OH^- \quad (4)$$

$Al(OH)_3$ is solid solvated into the $Ni(OH)_2$ lattice, therefore, the pH value is a key dynamic factor controlling the formation of $Ni(OH)_2$ and affecting its structure and electrochemical performance. In this section, the molar ratio of Al to (Ni + Al) is the same (20%).

The XRD patterns of the samples synthesized at different pH values are displayed in Fig. 1. The prominent phase of all samples is α phase and small percentage of β phase also appears at pH 11.0 and 12.25. During the precipitation process, the initial substance of Al exists as $AlO_2{}^-$. When pH is too high or low, large amounts of $AlO_2{}^-$ remains as $AlO_2{}^-$ or Al^{3+} in the solution, there is no enough Al^{3+} substitution for Ni position in the $Ni(OH)_2$ lattice, so the β phase can be formed.

Fig. 2 shows the effects of pH value on the tapping density of $Ni(OH)_2$ powders. The tapping density increases at first and then decreases with the increase of pH value. The highest

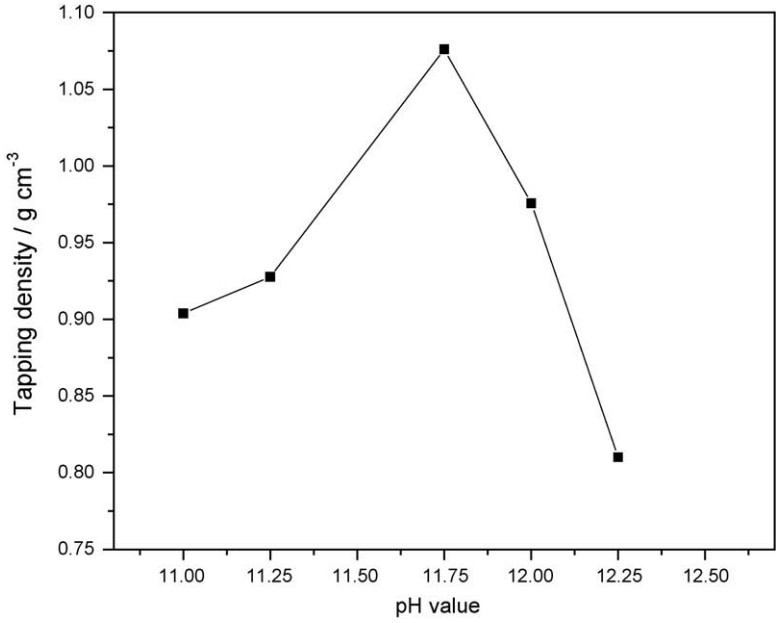

Fig. 2. The effects of pH value on the tapping density of Al-substituted α-$Ni(OH)_2$ (Al 20%).

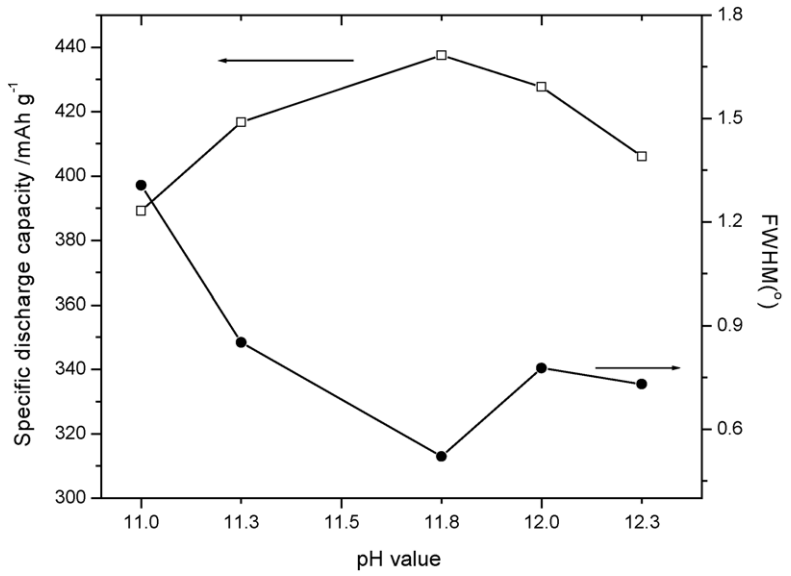

Fig. 3. The effects of pH value on the discharge capacity and FWHM of (0 0 3) plane of the Al-substituted α-Ni(OH)$_2$ samples (Al 20%).

tapping density of the sample is obtained at pH 11.75. The tapping density is directly determined by the nucleation rate of Ni(OH)$_2$ particle. When pH is too low, the precipitate cannot be obtained over a long period of time, and a large number of crystal nuclei are suddenly produced at the moment when the solubility of the precipitate is reached, then the sample with low density is obtained. On the contrary, when pH is too high, high relative supersaturation of the solution leads to the sample with low density. The highest tapping density prepared by this method is 1.1 g cm^{-3}, which is much lower than that of β-Ni(OH)$_2$ [1]. The Al-substituted α-Ni(OH)$_2$ shows a turbostatic character and a large interlayer distance. Therefore, the density of α-Ni(OH)$_2$ is lowered. But there is large space to increase its density through the optimization of technical conditions.

Fig. 3 shows the effect of pH value on the initial specific discharge capacity (per gram of pure Ni(OH)$_2$) and FWHM of (0 0 3) planes of the samples. It can be seen that the discharge capacity also shows a parabola trend with increasing pH value. However, the FWHM changes in the opposite direction. This clearly indicates that for α-Ni(OH)$_2$ the discharge capacity increases as the crystallinity is improved.

The above results indicates that the optimal pH value is 11.75 in terms of the tapping density and initial specific discharge capacity of the Ni(OH)$_2$ samples when the molar ratio of Al to (Al + Ni) in the synthesis solution is 20%. In order

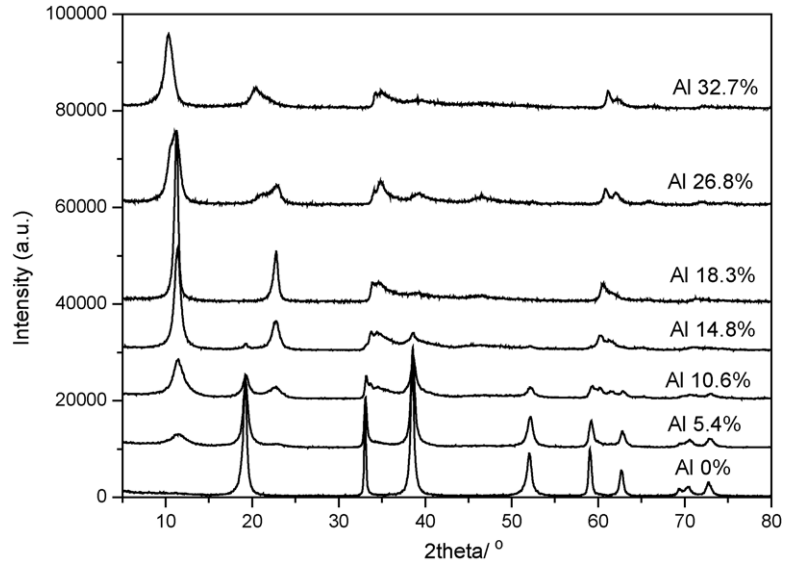

Fig. 4. XRD patterns of nickel hydroxide samples with different Al contents.

to discuss the effects of Al content on the physicochemical properties of the samples, the pH value is fixed at 11.75 in the following preparation.

3.2. Effects of Al content on the character of structure and morphology

3.2.1. XRD

The samples with different Al contents are named as Al C% (C is the molar percentage of Al to Ni and Al). Several typical XRD patterns of nickel hydroxide powders with different Al contents are displayed in Fig. 4. There is no peaks indicative of Al or $Al(OH)_3$ in these patterns, which implies that Al has coprecipitated with Ni into the $Ni(OH)_2$ lattice and substitutes for the Ni position. The nickel hydroxide without Al shows a typical structure of β-$Ni(OH)_2$. When 5.4% Al is added, the peak at $2\theta = 11.48^\circ$ appears, which is the characteristic of α-$Ni(OH)_2$, but the content of α phase is very low. After the Al content reaches 14.8%, the α phase plays a prominent part in the structure although some weak peaks of β phase are still maintained and the crystallinity of α phase becomes relatively high. When Al content is more than 18.3%, the $Ni(OH)_2$ manifests a pure α phase structure. It can be seen that the Al content has a strong effect on the formation and the crystallinity of stabilized α-$Ni(OH)_2$. The calculated cell constants (*a* and *c*) and the interlayer distance are listed in Table 1. It shows that the cell constant, *a*, decreases with increasing Al content in the nickel hydroxide, which is caused by the smaller ionic radius of Al^{3+}(0.54 Å) compared to Ni^{2+}(0.69 Å) in the lattice [18]. However, the interlayer distance and the cell constant, *c*, are both increased. The higher the Al content is, the more Ni positions in the lattice are substituted. Therefore, more positive charge is produced and more anions such as SO_4^{2-} and CO_3^{2-} are intercalated into the interlayer to compensate the positive charge.

Table 1
The cell constant *a* and *c* values and $d_{(003)}$ or $d_{(001)}$ of the samples

	a (Å)	*c* (Å)	$d_{(003)}$ or $d_{(001)}$ (Å)
Al 0% (β)	3.126	4.605	4.619
Al 5.4% (β)	3.123	4.603	4.604
Al 10.6% (α)	3.077	23.310	7.432
Al 14.8% (α)	3.079	23.258	7.756
Al 18.3% (α)	3.057	23.489	7.838
Al 26.8% (α)	3.044	23.162	7.838
Al 32.7% (α)	3.027	25.993	8.532

The XRD patterns of Al 32.7% and Al 26.8% samples show bad crystallinity, which indicates that the disorder degree of packing along *c* axis is increased due to the intercalation of large amounts of water molecules and anions.

Fig. 5 shows the XRD patterns of Al 18.3% sample after ageing in 6 M KOH at 45 °C for a week and at room temperature for 3 months. After ageing treatment at 45 °C for a week, the α phase is still maintained and the peak at about 60° clearly splits into two peaks. This condition is very strict for usage in actual Ni-MH batteries. So the excellent stability of Al-substituted α-$Ni(OH)_2$ at high temperature will not obstruct its use in commercial batteries. Unfortunately, after ageing at room temperature for 3 months, the peak of (0 0 1) indicative of β phase appears, but its intensity is very weak. The peaks of (0 0 3) and (0 0 6) become sharper, which indicates that the crystallinity of α-$Ni(OH)_2$ is improved and the turbostatic character is reduced.

3.2.2. SEM

Fig. 6 shows the SEM photos of Al 0%, Al 18.3% samples and Al 18.3% sample after ageing in 6 M KOH for 3 months at room temperature at different magnifications. At 1000 magnification, Al 0% sample appears as aggregates of several spherical and quasi-spherical particles and the uni-

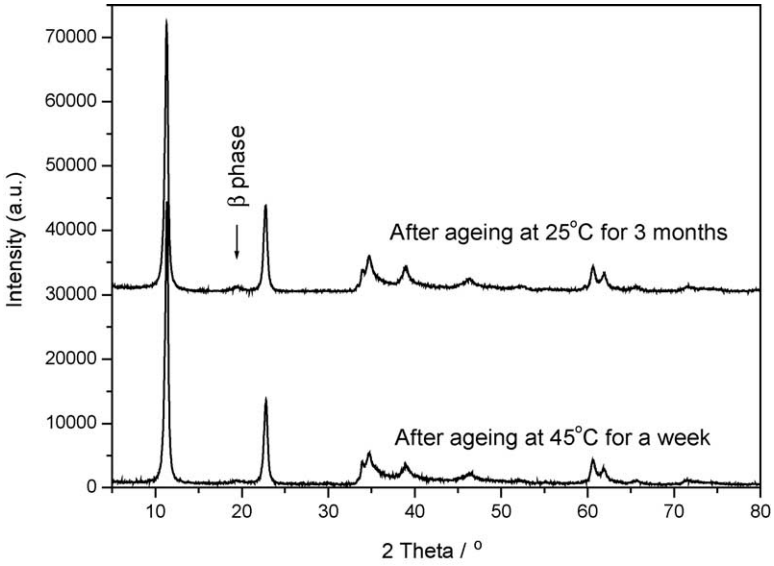

Fig. 5. XRD patterns of Al 18.3% sample after ageing treatment.

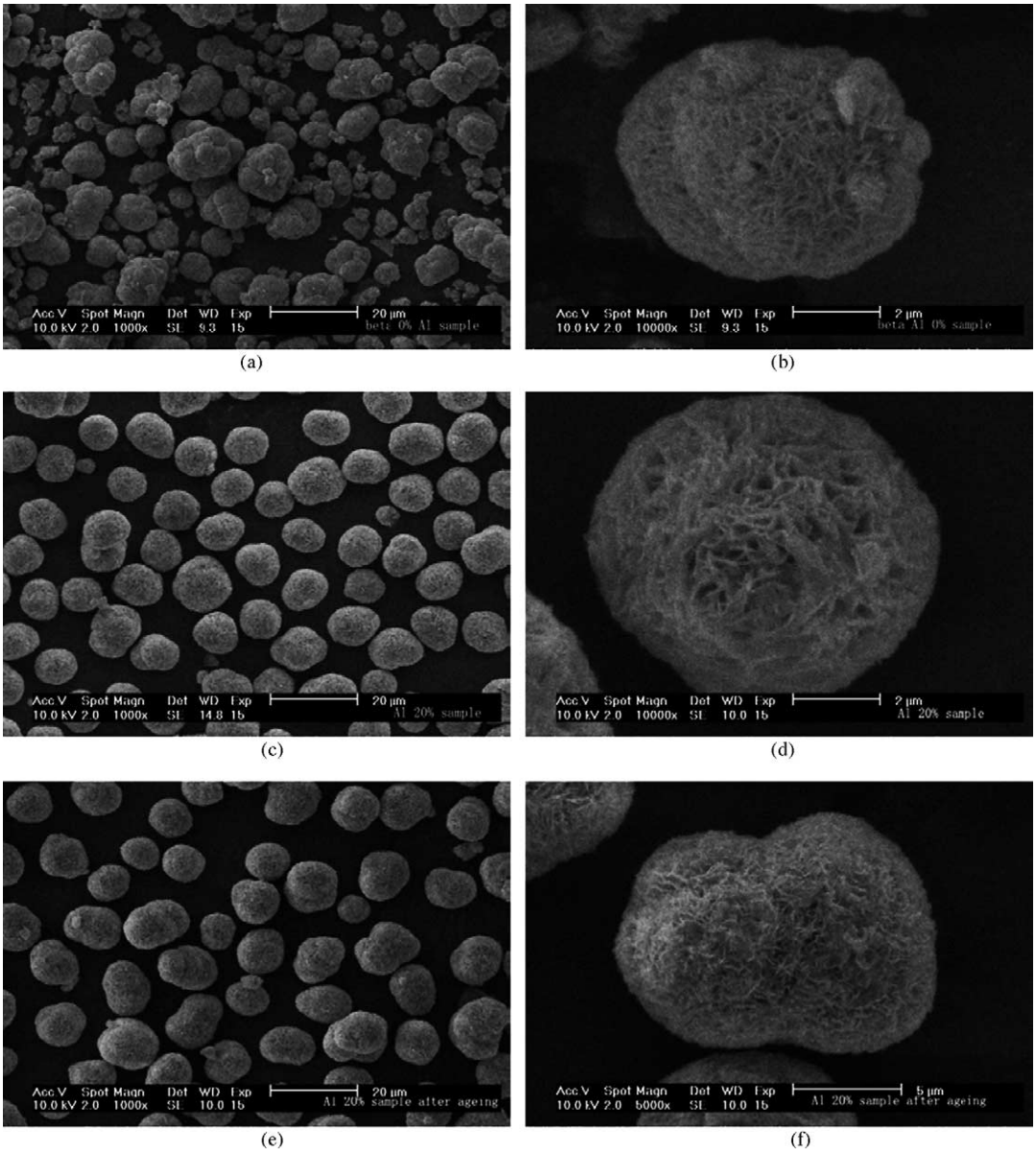

Fig. 6. SEM photos of samples, (a) and (b): Al 0% sample; (c) and (d): Al 18.3% sample; (e) and (f): Al 18.3% sample after ageing for 3 months at room temperature.

formity of particle size is very low. However, the Al 18.3% sample shows the perfect spherical particles and the size is almost uniform without the aggregate of particles. As we know, the Al-substituted α-$Ni(OH)_2$ almost has no definite shape or shows aggregates of thin crumpled sheets [6,7]. The spherical particles are resulted from the complexation-coprecipitation preparation method, which accelerates the even agglomeration of crystallite from all the directions and forms a typical spherical particle. Spherical particle has good fluidness and is easier to be filled into the foam nickel than irregular particles during the manufacture of batteries. At high magnification, the crossed agglomerations of crystallites can be seen on the surface of particles for both Al 0% and Al 18.3% samples. More defects appear and the connection between crystallites is more looser for Al 18.3% sample, which increases the specific active area and also results in the low tapping density of α-$Ni(OH)_2$.

The aged sample shows the conglomeration of three or more spherical particles. Fig. 6(f) clearly shows the growth of particles through the connection between crystallites of different particles. In the ageing process, small particles are dissolved and large particles become more and more larger. Wang et al. [9] also reported that a recrystallization process occurs with alkaline ageing treatment which causes growth of crystalline size and a loss of turbostatic disorder.

AAS and ICP results show that the Al content of Al 18.3% sample after ageing treatment for 3 months at room temperature is 18.0%, which can be considered to be almost un-

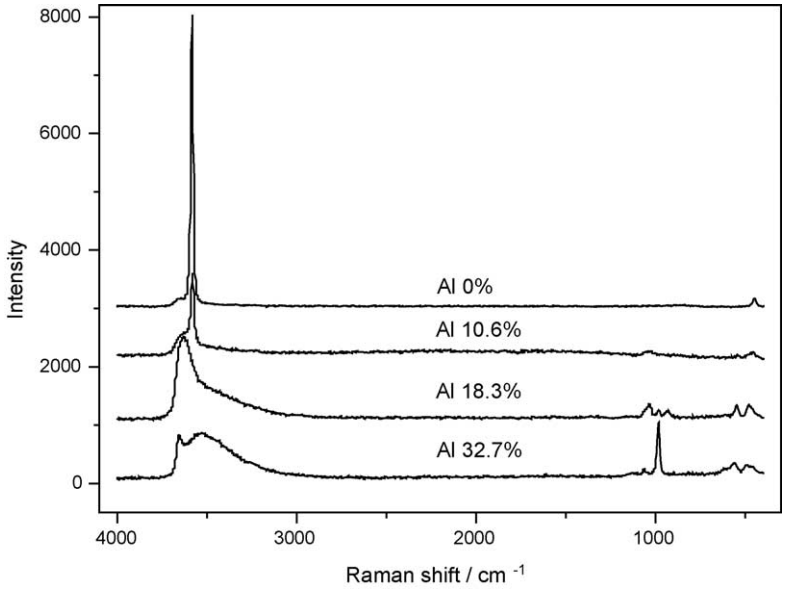

Fig. 7. Raman spectra of nickel hydroxides with different Al contents.

changed. However, for Zn-substituted α-Ni(OH)$_2$, a large amount of Zn is lost during ageing in KOH and oxidation reactions [14]. The Zn/(Zn + Ni) molar ratio of $\alpha_{25\%\,Zn}$ sample decreased from 25% to 4% after ageing in 8 M KOH for a week at room temperature. Compared with Zn, the Al element coprecipitated in nickel hydroxide lattice is more stable and difficult to solve in the alkaline solution although Al belongs to amphoteric metals, which is probably resulted from the different positions of Al and Zn in Ni(OH)$_2$ lattice. In Al-substituted α-Ni(OH)$_2$, Al occupies the Ni positions, however, for Zn-substituted sample, a large amount of Zn still stays in the interslab space of NiO_2 layers [13].

3.2.3. Raman spectroscopy

Fig. 7 shows the Raman spectroscopy of the nickel hydroxide samples. The sharp and strong peaks at 3580 cm^{-1} of Al 0% and Al 10.6% samples are attributed to the symmetric stretch of the free hydroxide groups of the crystalline bulk. However, for Al 18.3% samples, the symmetric stretch of the hydroxide groups appears at 3630 cm^{-1}, which is probably caused by the hydrogen bonding of OH with the interlay water and anions [5,6]. The Raman peak at about 3600 cm^{-1} splits into two peaks at 3660 and 3530 cm^{-1} for the Al 32.7% sample, which indicates that there are both free and hydrogen bonded OH. Sev-

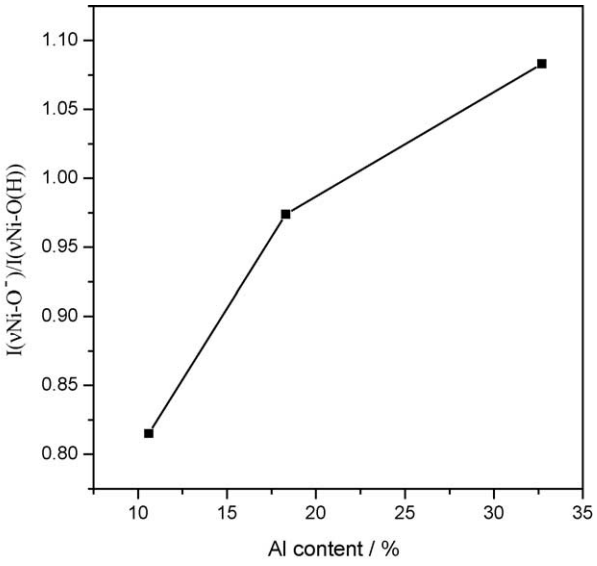

Fig. 8. The effect of Al content on the intensity ratio of νNi─O$^-$ to νNi─O(H).

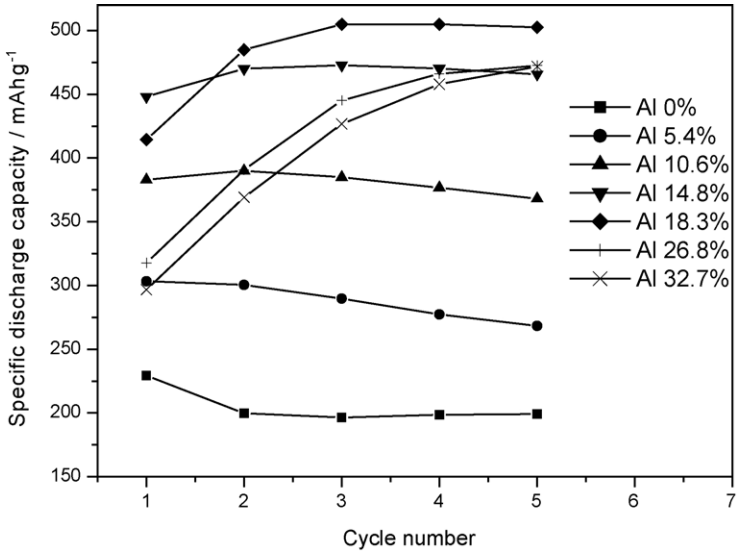

Fig. 9. The activation behavior of $Ni(OH)_2$ with different Al contents.

eral peaks at 1040–900 cm^{-1} are observed for Al-substituted α-$Ni(OH)_2$, which is the character of the intercalated anions such as SO_4^{2-} and CO_3^{2-}, compensating the excess positive charge caused by the substitution of Al^{3+} for Ni^{2+}.

A band at 448 cm^{-1} is observed on the Raman spectrum of Al 0% sample, which can be assigned to the Ni–O stretching vibration of Ni^{2+} species associated with OH groups (νNi–O(H)) [19,20]. The νNi–O(H) of Al 18.3% and Al 32.7% samples appear at 479 and 489 cm^{-1}, respectively. It can be seen that the peak of νNi–O(H) shifts to higher frequency with increasing Al content. Another kind of peaks are also observed at 547 and 566 cm^{-1} for Al 18.3% and Al 32.7% samples respectively, which can be attributed to the Ni–O stretching vibration of Ni^{2+} species associated with O^{2-} (νNi–O^-) [19,20], indicating of proton vacancy sites. The νNi–O^- peak is also shown in Al 10.6% sample at 545 cm^{-1}, but it is very weak. Fig. 8 displays the effect of Al content on the intensity ratio of νNi–O^- to νNi–O(H). It can be clearly seen that the proton vacancy is increased by the substitution of Al for Ni position in $Ni(OH)_2$ lattice and the insertion of Al^{3+} cation in the nickel hydroxide lattice creates proton vacancy. The excess positive charge caused by the doping of Al^{3+} is compensated by the insertion of anions such as SO_4^{2-} and CO_3^{2-} and the formation of proton defects. The occur-

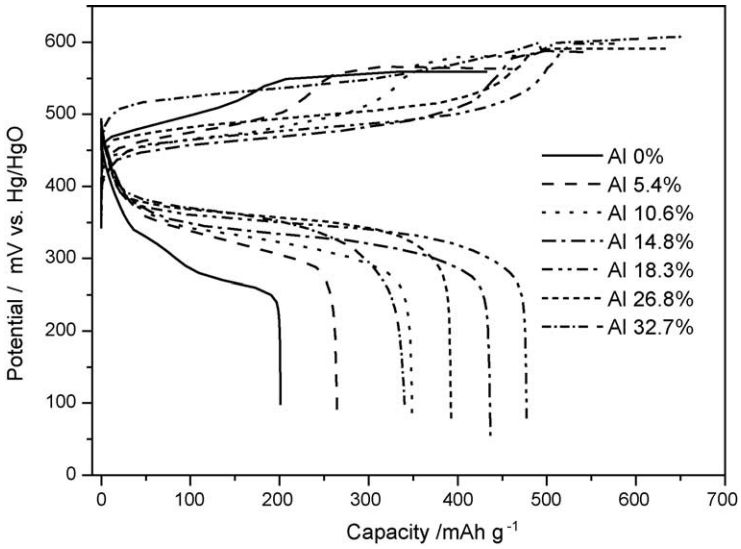

Fig. 10. The first charge–discharge curves of $Ni(OH)_2$ with different Al contents at 1.0 C rate.

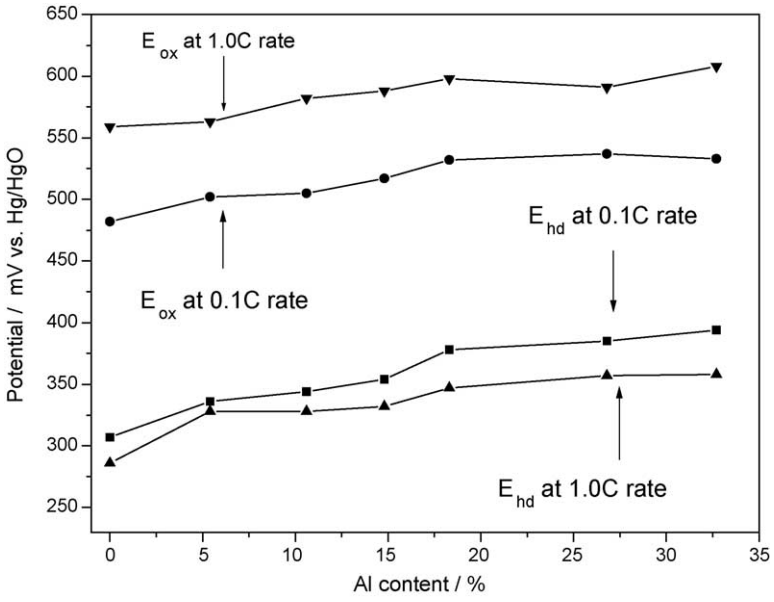

Fig. 11. The E_{hd} and E_{ox} of the samples with different Al contents at different rates.

rence of proton defects can increase the diffusion coefficient of proton, which will be verified in the following section.

3.3. Effects of Al content on the electrochemical performance

3.3.1. Activation performance

Fig. 9 shows the activation behavior at 0.1 C rate of the nickel hydroxide electrodes. It can be seen that with the increase of Al content the activation of the active materials becomes more difficult. For Al 0% and Al 5.4% samples, the discharge capacity reaches the maximum at the first activation process and then decreases in the following activation procedure, which means that there is no need for activation for these samples. For Al 10.6%, Al 14.8% and Al 18.3% samples, the discharge capacity reaches the maximum at the second or the third activation cycling. For α-$Ni(OH)_2$ with high Al content (26.8%, 32.7%), the discharge capacity continuously increases during the activation process. It can be

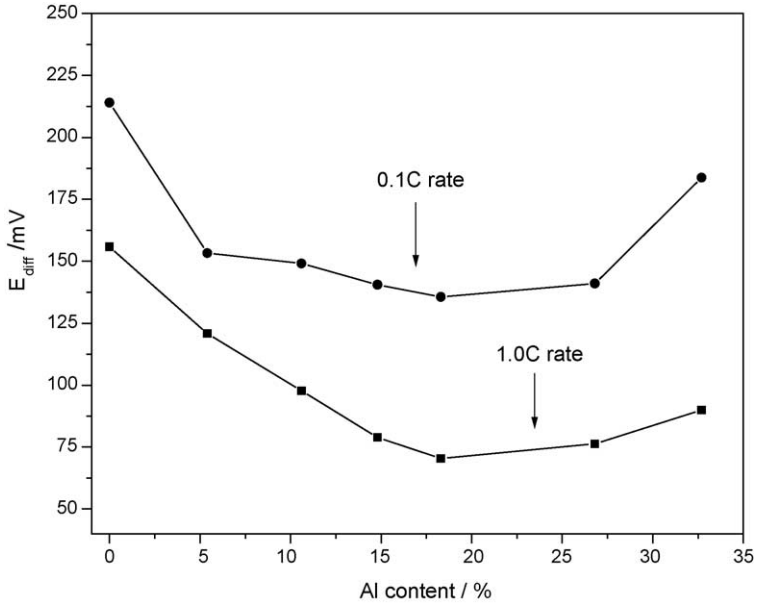

Fig. 12. The E_{diff} of the samples with different Al contents at different rates.

concluded that the α-phase $Ni(OH)_2$ is more difficult to activate than β-phase sample.

3.3.2. Galvanostatic charge–discharge

Fig. 10 shows the charge–discharge curves of nickel hydroxide electrodes with different Al contents at 1.0 C rate. The Al-substituted $Ni(OH)_2$ electrode shows a stable potential over a long duration after an initial fast decease of potential, which represents a perfect discharge plateau. The discharge curve of $Ni(OH)_2$ without Al has a relatively less stable potential duration compared with Al-substituted α-$Ni(OH)_2$ samples. Fig. 11 shows the effects of Al content on the oxygen evolution potential (E_{ox}) and half discharge potential (E_{hd}, defined as the potential at the half discharge capacity) at 0.1 and 1.0 C rates. E_{ox} increases slowly and E_{hd} increases markedly with the increase of Al content at all charge–discharge rates. The E_{hd} of Al 32.7% sample is 87 mV higher than that of Al 0% sample at 0.1 C rate.

Barnard et al. [3] reported that the α/γ system has a lower reversible potential compared with β/β system, where the α-$Ni(OH)_2$ without any doped metal ions is pure and the α phase is labile. But for metal substituted α-$Ni(OH)_2$, the type and content of the doped metal have strong influence on the potential of α-$Ni(OH)_2$ electrodes. Based on the difference in size between the substitution cation and the nickel ion in the γ phase, a model has been proposed by Guerlou-Demourgues and Delmas [12] to explain the effect of the substituting cation on the potential of nickel hydroxide electrode. It explains quite well the observed effect of Mn-, Co-, Fe-substituted nickel hydroxide. The smaller size of the Mn^{4+} ion ($rMn^{4+} = 0.54$ Å) against that of Ni^{3+} one ($rNi^{3+} = 0.56$ Å) induces a decrease in the electrode potential with increasing substitution amount, similarly for the cobalt system, whereas in the case of the Fe-substituted material the larger size of the Fe^{3+} and Fe^{4+} ions ($rFe^{3+} = 0.64$ Å and $rFe^{4+} = 0.59$ Å) entails an increase in the potential. But the potential of Al-substituted $Ni(OH)_2$ is not decreased due to the smaller radii of Al^{3+} ($rAl^{3+} = 0.54$ Å) than that of Ni^{3+}. During our research, we also found that the discharge potential of Zn-substituted α-$Ni(OH)_2$ decreased with increasing Zn content, however, the radii of Zn^{2+} ($rZn^{2+} = 0.74$ Å) is larger than that of Ni^{3+}. In the case of Al, a hypothesis, based on the hybridization of metal-oxygen atomic orbitals, was recently proposed to explain the experimental increase of the electrode potential in the $LiCo_{1-y}Al_yO_2$ layered system [21]. For the late-transition-metal oxides, the oxygen is in large part responsible for the electron exchange. The electron exchange with oxygen leads to a lower electrostatic energy (hence a higher potential), which can be speculated that the increased potential correlates with the increased oxygen participation in the electron exchange. Similarly, the participation of oxygen during the electron exchange is quite possible in the Al-substituted α-$Ni(OH)_2$ electrodes.

The difference (E_{diff}) between E_{hc} (defined as the potential at the half charge capacity before reaching the plateau of oxygen evolution) and E_{hd} is the characteristic of the electrode polarization degree. Fig. 12 shows the E_{diff} of the samples with different Al contents at 0.1 and 1.0 C rates. It is obvious that E_{diff} decreases with the increase of Al content and then increases slowly. E_{diff} reaches the minimal value at Al 18.3% sample, which indicates the minimal polarization in the electrode reaction. The reason why the E_{diff} changes with the Al content will be explained by the following tests of the diffusion coefficient of proton.

3.3.3. Tests of the diffusion coefficient of proton (D_{H^+})

In order to verify the trend of the diffusion, the diffusion coefficient of proton (D_{H^+}) was measured by current pulse relaxation (CPR) method. The closed-circuit potential and quasi-equilibrium open-circuit potential are presented in Fig. 13(a) as a function of discharge capacity for Al 18.3% sample. When the current is interrupted after discharging to various capacities, the potentials of the nickel electrode recover gradually towards the equilibrium state. This is caused by a slow diffusion of protons from the electrode surface towards the bulk [15–17]. A typical transient voltage (ΔE) in Al 18.3% sample observed after the passage of a current pulse at 66.7% depth of discharge (DOD, the ratio of the actual discharge capacity at different conditions to the actual discharge capacity discharging to 0.1 V versus Hg/HgO) is plotted against $t^{-1/2}$ in Fig. 13(b). The slope of the linear region can be used to calculate the diffusion coefficient of protons, D_{H^+}, in the nickel hydroxide electrodes using Eq. (1).

Fig. 14 shows the D_{H^+} values of Al 0%, 10.6%, 18.3%, 32.7% samples at different DOD. The D_{H^+} of Al-substituted sample is much higher than that of pure β-$Ni(OH)_2$. The interlayer distance of α-$Ni(OH)_2$ is much more than that of β-$Ni(OH)_2$ shown in XRD results and many proton defects are formed in α-$Ni(OH)_2$ as indicated by the former Raman spectroscopy, which makes the diffusion of H^+ much easier. When the Al content is too high (such as 32.7%), the intercalated anions such as SO_4^{2-} and CO_3^{2-} obstruct the transportation of H^+ in the interslab. Thus the D_{H^+} is decreased. The change of D_{H^+} explains well the former results of E_{diff}. Al 18.3% sample has the highest D_{H^+} and lowest E_{diff}, which decreases the diffusion polarization of the electrode process. For a certain Al-substituted sample, D_{H^+} increases first and then decreases, and at a certain DOD, it reaches the maximum value. The same inclination of D_{H^+} with DOD was also observed in our previous work [22].

3.3.4. The cycle performance of the nickel electrodes

Fig. 15 shows the cycle life of the electrodes at 1.0 C rate using nickel hydroxide samples with different Al contents as active material. The specific discharge capacity is in terms of the capacity per gram of pure $Ni(OH)_2$. At the first cycle, the Al 18.3% sample has the highest specific discharge capacity, 477 mAh g^{-1}, which corresponds to 1.65 electron transfer. The sample without Al shows the lowest discharge capacity and its highest discharge capacity is only 268 mAh g^{-1}, which corresponds to 0.93 electron transfer.

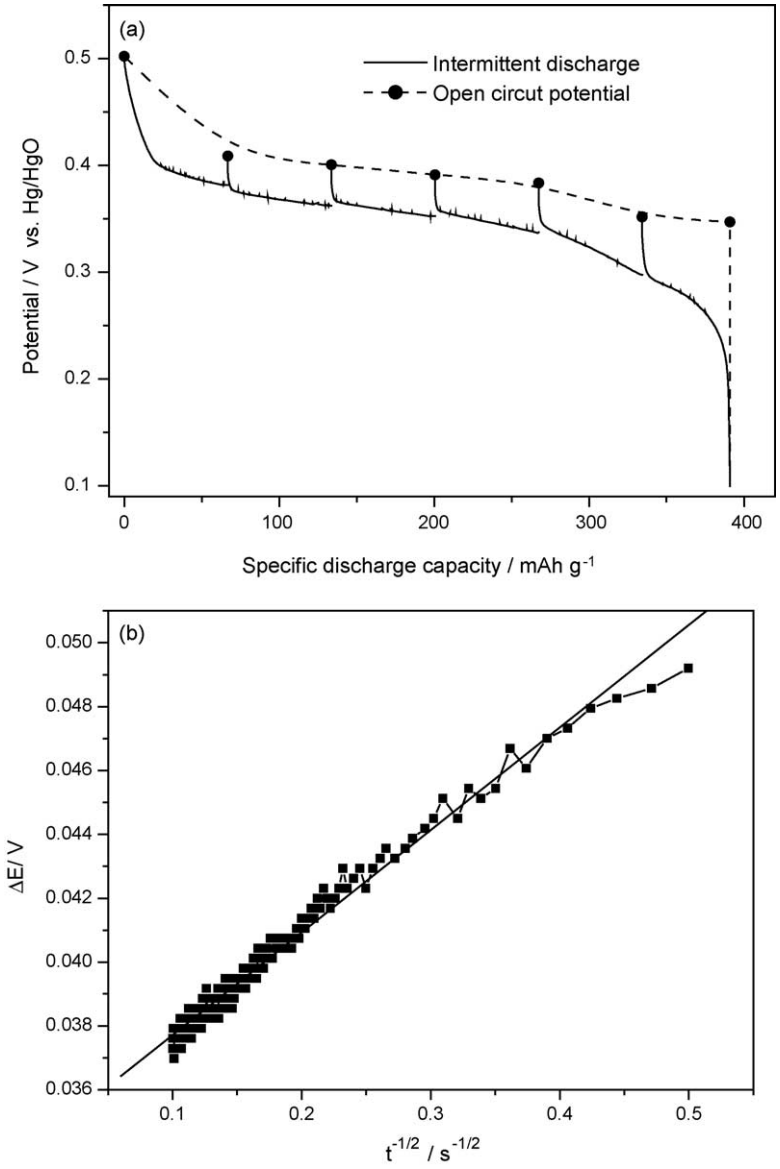

Fig. 13. (a) Closed-circuit and open-circuit potentials as a function of discharge capacity of Al 18.3% sample and (b) typical plot of observed voltage (ΔE) against $t^{-1/2}$ for Al 18.3% sample at 66.7% DOD.

More than one electron transfer per Ni atom can be obtained during α-$Ni(OH)_2$/γ-NiOOH transformation because the oxidation state of Ni in γ-NiOOH is 3.3–3.67 [2,3] due to the existence of Ni^{4+}. However, the oxidation state of Ni in β-NiOOH is less than 3.0. Therefore, the α/γ couple has more electron transfer and much higher discharge capacity than β/β couple.

At the first cycle, the discharge capacity increases and then decreases with increasing the Al content. It reaches the maximum value at Al 18.3% sample. Considering the former XRD results, the percentage of α phase in the total nickel hydroxide sample increases with the increase of Al content, which leads to increasing the oxidation state of Ni in the charge states. When the content of Al is more than 18.3%, it is difficult to charge due to the high charge potential as shown in Fig. 10. Therefore, the discharge capacities of Al 26.8% and Al 32.7% samples decrease quickly.

During the initial 150 charge–discharge cycles, the discharge capacity of Al-substituted $Ni(OH)_2$ except for Al 32.7% sample fades fast, and then maintains at a relatively high level even till the 600th cycle. However, the discharge capacity of $Ni(OH)_2$ without Al decreases quickly after 300 cycles. At the 600th cycle, the discharge capacity of $Ni(OH)_2$ without Al is still much lower than those of Al-substituted $Ni(OH)_2$ electrodes. It is very interesting that the discharge capacity of Al 32.7% sample is tremendously stable from the first cycle to the 600th cycle. Its deterioration rate of capacity is only 7% at 600th cycle, which is likely resulted from the contribution of high Al substitution content on the structural and electrochemical stability of α-$Ni(OH)_2$.

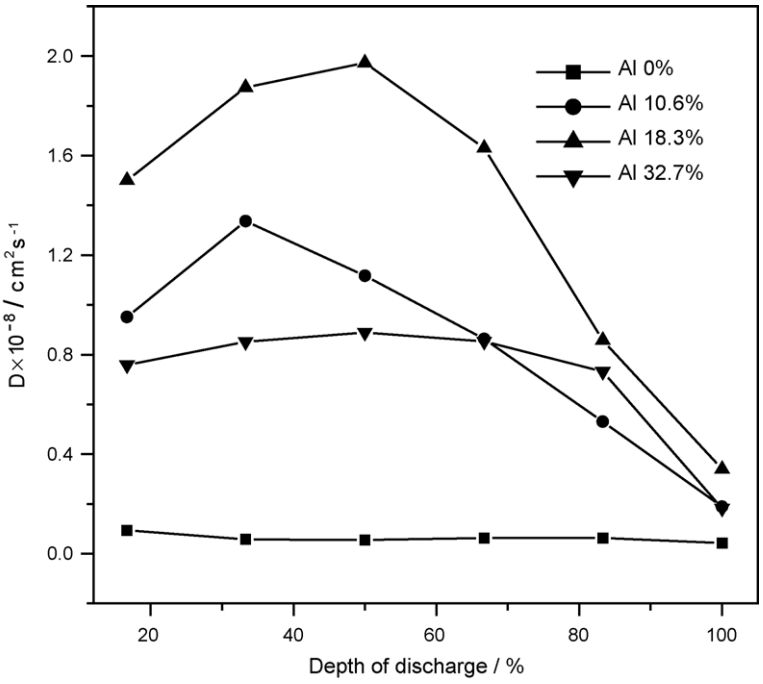

Fig. 14. DOD dependence of proton diffusion coefficient for different samples.

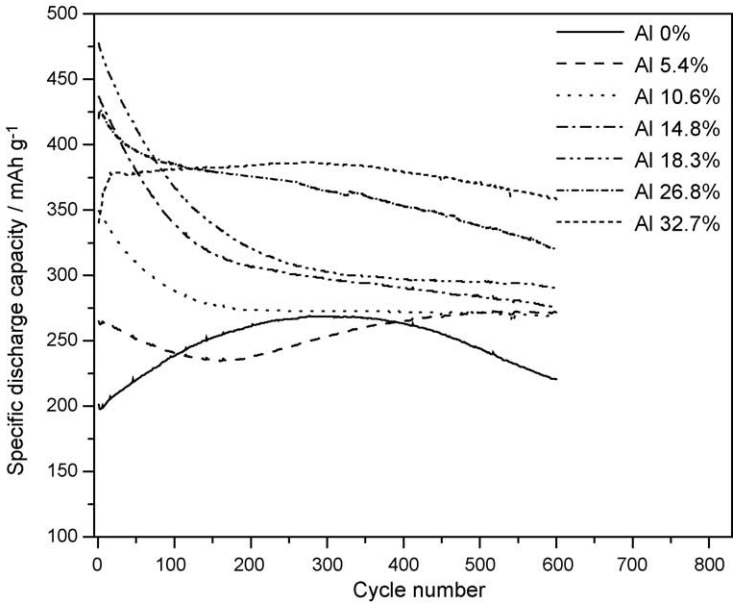

Fig. 15. The cycle performance of the samples with different Al contents at 1.0 C rate.

4. Conclusion

1. The spherical Al-substituted α-$Ni(OH)_2$ samples for alkaline rechargeable batteries were prepared by a complexation-coprecipitation method. The optimal pH value is 11.75 in terms of the tapping density and initial discharge capacity of the $Ni(OH)_2$ samples when the molar ratio of Al to (Ni + Al) in the synthesis solution is 20%.
2. The specific discharge capacity of Al-substituted α-$Ni(OH)_2$ increases with increasing Al content and it reaches 477 mAh g^{-1} when the Al content is 18.3%, which is much higher than that of β-$Ni(OH)_2$ without Al substitution. The oxygen evolution potential and the half discharge potential increase greatly with the increase of Al content. The capacity stability during 600 charge–discharge cycles is improved by large amount substitution of Al, however,

Al-substituted α-$Ni(OH)_2$ is more difficult to activate than β-$Ni(OH)_2$.

3. Compared with β-$Ni(OH)_2$, there are large amounts of proton defects and long interlayer distance in Al-substituted α-$Ni(OH)_2$ which increases the diffusion coefficient of proton measured by current pulse relaxation (CPR) and decreases the diffusion polarization. The Al-substituted α-$Ni(OH)_2$ sample shows excellent structural stability during ageing treatment in 6 M KOH solution and the loss of Al can be neglected.

Acknowledgements

This work was supported by National Natural Science Foundation of China (Approval No. 59902004). The authors also gratefully acknowledge the financial support of the Chinese State Key Laboratory for Corrosion and Protection.

References

[1] H. Bode, K. Dehmelt, J. Witte, Electrochim. Acta 11 (1966) 1079.
[2] D.A. Corringan, S.L. Knight, J. Electrochem. Soc. 136 (1989) 613.
[3] R. Barnard, C.F. Randell, F.F. Tye, J. Appl. Electrochem. 10 (1980) 109.
[4] C. Faure, C. Delmas, P. Willmann, J. Power Sources 36 (1991) 497.
[5] P.V. Kamath, M. Dixit, L. Indira, J. Electrochem. Soc. 141 (1994) 2956.
[6] A. Sugimoto, S. Ishida, K. Hanawa, J. Electrochem. Soc. 146 (1999) 1251.
[7] B. Liu, X.Y. Wang, H.T. Yuan, Y.S. Zhang, D.Y. Song, Z.X. Zhou, J. Appl. Electrochem. 29 (1999) 855.
[8] Y.J. Leng, B. Liu, F.J. Wang, J.X. Zhou, Y. Xiao, Z.F. Ma, Chin. J. Power Sources 24 (2000) 326.
[9] C.Y. Wang, S. Zhong, K. Konstantinov, G. Walter, H.K. Liu, Solid State Ionics 148 (2002) 503.
[10] W.-K. Hu, D. Noreus, Chem. Mater. 15 (2003) 974.
[11] L. Guerlou-Demourgues, C. Delmas, J. Power Sources 45 (1993) 281.
[12] L. Guerlou-Demourgues, C. Delmas, J. Electrochem. Soc. 143 (1996) 561.
[13] C. Tessier, L. Guerlou-Demourgues, C. Faure, M. Basterreix, G. Nabias, C. Delmas, J. Mater. Chem. 10 (2000) 1185.
[14] C. Tessier, L. Guerlou-Demourgues, C. Faure, M. Basterreix, G. Nabias, C. Delmas, Solid State Ionics 133 (2000) 11.
[15] N. Kumagai, S. Tanifuji, T. Fujiwara, K. Tanno, Electrochim. Acta 37 (19921039).
[16] K. Watanabe, T. Kikuoka, J. Appl. Electrochem. 25 (1995) 219.
[17] K. Watanabe, M. Koseki, N. Kumagai, J. Power Sources 58 (1996) 23.
[18] J.A. Dean, Lange's Handbook of Chemistry, 15th ed., McGraw-Hill, New York, 1999, p. 4.29.
[19] S. Deabate, F. Fourgeot, F. Henn, J. Power Sources 87 (2000) 125.
[20] M.C. Bernard, R. Cortes, M. Keddam, H. Takenouti, P. Bernard, S. Senyarich, J. Power Sources 63 (1996) 247.
[21] G. Ceder, Y.-M. Chiang, D.R. Sadoway, M.K. Aydinol, Y.-I. Jang, B. Huang, Nature 392 (1998) 694.
[22] H. Chen, J.M. Wang, T. Pao, Y.L. Zhao, J.Q. Zhang, C.N. Cao, J. Electrochem. Soc. 150 (2003) 1399.